

Broadband second harmonic generation using total internal reflection-quasi phase matching in a multi-tapered isotropic semiconductor slab

P. DEBNATH, S. DEB*

Department of Electrical Engineering, National Institute of Technology, Agartala, Barjala, Jirania, Tripura (west), Pin-799046, Tripura, India

This paper analytically explores the possibility of broad bandwidth (BW) as well as high conversion efficiency of second harmonic generation in a multi-tapered isotropic semiconductor slab made of zinc telluride (ZnTe) and cadmium telluride (CdTe), using total internal reflection-quasi phase matching technique. A computer aided simulation has been executed where efficiency of 11.34 % with a 3 dB BW of 426 nm, centered at 10.737 μm and 22.37 % with a 3 dB bandwidth of 346 nm, centered at 7.85 μm has been obtained in a ZnTe and CdTe slab respectively of 10 mm slab length. Moreover, the effect of different conversion yield limiting factors along with that of the nonlinear law of reflection has also been taken into consideration.

(Received May 05, 2016; accepted August 9, 2017)

Keywords: Total internal reflection-quasi phase matching, Zinc telluride, Cadmium telluride

1. Introduction

Now-a-days broadband optical sources attract applications in different context in various fields like physics, acoustics, optical communication, radio systems engineering, telecommunication, etc. Broadband second harmonic generation (SHG) is a technique where the second harmonic light will be generated over a wide spectral range due to nonlinear interaction in an appropriate $\chi^{(2)}$ medium. However, the output of this process is generally poor, because of the phase mismatch among the interacting waves. In order to solve this problem quasi phase matching (QPM) may be considered as a suitable method in frequency conversion which can be achieved by periodic poling of the nonlinear crystalline material such as lithium niobate (LiNbO_3), lithium tantalate (LiTaO_3) and potassium titanyl phosphate (KTiOPO_4) [1-2].

In SHG, certain isotropic semiconductor materials (GaAs, ZnSe etc) are found compatible using to their high optical second-order nonlinear susceptibility, good mechanical features, excellent transparency over 1-15 μm range, etc [3]. In single-crystalline materials, the main factor for an efficient optical conversion is coherence length Λ_c , i.e., the distance over which the relative phase lag of the three waves add up to π [4]. However, because of the phase mismatch, repeated build up and decline of radiation is observed. Therefore, QPM is used where the crystal axes are flipped by π allowing the energy to continuously getting extracted from the pump, and the SH field grows monotonically [5].

QPM using total internal reflection (TIR) in a plane parallel slab was first demonstrated by Armstrong et al. [6]

which was then used in different isotropic semiconductors (GaAs, ZnSe, ZnS) by a number of relevant researchers [7-9].

In this paper, we have analytically exhibited broadband SHG in a multi-tapered isotropic semiconductor slab made of ZnTe and CdTe, using TIR-QPM technique. With the help of simple geometry, the variation of proposed slab dimensions has been considered. The conversion efficiency and 3 dB bandwidth (BW) has been obtained with the help of MATLAB based simulation. Some of the factors like surface roughness, Goos-Hänchen (GH) shift, linear absorption as well as the effect of destructive interference due to nonlinear law of reflection when added to the analysis resulted in a reduced efficiency. The dependability of SHG conversion efficiency and its BW have been studied for different slab lengths, and different vertical heights.

2. Proposed Scheme

For broadband SHG we have proposed a multi-tapered isotropic semiconductor slab configuration AGBCMD of length, $L = 10$ mm and thickness, $t = 400$ μm as shown in Fig. 1. Here, the upper surfaces GR and GT are tapered at an angle of θ_1 and θ_3 respectively. Similarly the lower surfaces MP and MU are tapered at an angle of θ_2 and θ_4 respectively. The angles are determined by the vertical heights of the two side ends of the slab i.e., $t_1 = 5$ μm , $t_2 = 6$ μm , $t_3 = 7$ μm and $t_4 = 8$ μm for ZnTe and $t_1 = 15$ μm , $t_2 = 16$ μm , $t_3 = 17$ μm and $t_4 = 18$ μm for CdTe respectively and the upper and lower surface lengths are L_1, L_2, L_3 and L_4 , where $L_2 = L_3 = L/2$ and L_1, L_4 (depends

on the functions of L, t, t_1, t_2, ψ) have been calculated using simple geometry. The face on which the beam of fundamental light has been made incident on the slanted slab side AD inclined at an angle $\psi = 0.7$ radian with respect to the vertical surface. The distance SP from the entrance point to the lower surface PM is $x = 190 \mu\text{m}$.

Let the fundamental laser radiation with centre frequency ω_1 is incident at an angle ϕ_i with respect to the normal on the inclined slab end face. The first angle of incidence ϕ_i has been determined by the refractive indices inside the slab corresponding to each wavelength available in the input broadband source using the Sellmeier's equation of the selected material i.e. ZnTe [10] and CdTe [11]. If ϕ_i is greater than the critical angle, TIR condition can be achieved. Therefore, the collimated optical radiation will experience multiple bounces throughout the slab length. Based on this slab configuration, two sections exist – (i) converging section GADM, where the bounce lengths are gradually decreasing till the mid section and (ii) diverging section GBCM, where the bounce lengths are gradually increasing till the end of the slab.

The proposed multi-tapered slab geometry provides the scope for wide variation in the interaction length of the interacting waves inside it. In case of a parallel slab [6], the slab thickness is optimized to have maximum conversion yield for SHG of a given input laser wavelength, minimizing the phase mismatch between the interacting waves. But since the proposed broadband SHG frequency converter converts a band of frequencies, rather than a single frequency, it is difficult to optimize the interaction length between successive bounces for each frequency available in the input broadband source. However, due to variation in interaction length, it may so happen that one interaction length between two successive bounces interaction length may coincide with an odd multiple of the coherence length for a particular frequency of the input broadband source, whereas another interaction length may coincide with an odd multiple of the coherence length of another frequency of the input broadband source and so on, thereby resulting in a flatter SH broadband output.

$$l_{\text{even}} = \left\{ \frac{D \sin \theta_2 \sin [(\phi_r + \psi) + (n-2)(\theta_1 + \theta_2)]}{\cos \phi_{n-1} \sin \left(\frac{\pi}{2} + \theta_2 - \phi_{n-1} \right)} + \frac{t}{\sin \left(\frac{\pi}{2} + \theta_2 - \phi_{n-1} \right)} + \frac{D_1 \sin \theta_1}{\cos \phi_n} \right\} \quad (6)$$

where, $n=2, 4, 6, \dots, n_{\text{tot}}$

n_{tot} indicates total number of bounces in the converging section of multi-tapered slab.

$$\phi_n = [\phi_{n+1} - (\theta_1 + \theta_2)] \quad (7)$$

where, $n=2, 4, 6, \dots, n_{\text{tot}}$

$$D = \left(L_1 - x \sin \psi - \frac{x \cos \psi}{\tan(\phi_r + \psi)} \right) \quad (8)$$

$$\theta_1 = \tan^{-1} \left(\frac{t_1}{L_4} \right) \quad (9)$$

2.1. Numerical analysis

In this multi-tapered slab (Fig. 1) with simple geometric calculation the generalized expressions for lengths between two successive bounces has been calculated as follows:

$$l_1 = \left[\frac{x \cos \psi}{\sin(\phi_r + \psi)} + \frac{\left(L_1 - x \sin \psi - \frac{x \cos \psi}{\tan(\phi_r + \psi)} \right) \sin \theta_2}{\cos \phi_i} \right] \quad (1)$$

where, l_1 is the 1st bounce length from the entrance point to the first TIR bounce point.

Now the angle of refraction in the denser medium, i.e., ϕ_r can be expressed as,

$$\phi_r = \sin^{-1} \left[\left(\frac{\sin \phi_i}{n_1} \right) \right] \quad (2)$$

where, n_1 is the refractive index corresponding to the input broadband source.

$$\theta_2 = \tan^{-1} \left(\frac{t_2}{L_1} \right) \quad (3)$$

$$L_1 = \left(\frac{L}{2} - t_2 \tan \psi \right) \quad (4)$$

and the first angle of incidence,

$$\phi_i = \left[\frac{\pi}{2} - (\theta_2 + \phi_r + \psi) \right] \quad (5)$$

Now for converging section, the even and odd bounce lengths can be expressed as follows:

$$L_4 = \left[\frac{L}{2} - (t + t_1 + t_2) \tan \psi \right] \quad (10)$$

$$D_1 = \left[D - \frac{D \sin \theta_2 \cos(\phi_r + \psi)}{\cos \phi_i} - \frac{D \sin \theta_2 \sin(\phi_r + \psi)}{\cos \phi_i \tan \left(\frac{\pi}{2} + \theta_2 - \phi_i \right)} - \frac{t}{\tan \left(\frac{\pi}{2} + \theta_2 - \phi_i \right)} \right] \quad (11)$$

$$l_{odd} = \left[\frac{D_1 \sin \theta_1 \sin \left(\frac{\pi}{2} + \theta_2 - \phi_{n-2} \right)}{\cos \phi_{n-1} \sin \left[(\phi_r + \psi) + (n-1)(\theta_1 + \theta_2) \right]} + \frac{t}{\sin \left(\frac{\pi}{2} + \theta_1 - \phi_{n-1} \right)} + \frac{D \sin \theta_2}{\cos \phi_n} \right] \quad (12)$$

where, $n=3, 5, 7, \dots, n_{tot}$

Now as the ray propagates from the converging section to the diverging section, we can be observed either of the 2 cases:

Case 1: If the ray, denoted by FK, is travelling from upper surface of the converging section to the lower surface of the diverging section (Fig. 1).

Case 2: If the ray, denoted by NH, is travelling from lower surface of the converging section to the upper surface of the diverging section (Fig. 2).

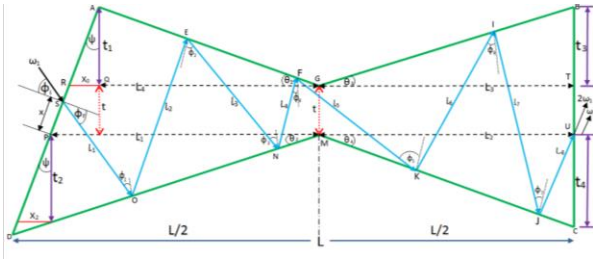


Fig. 1 Geometry of multi-tapered slab for Case 1

Case 1

$$l_{odd} = \left[\frac{z_0 z_1 z_2 z_3 \sin \theta_1 \sin \left(\frac{\pi}{2} + \theta_2 - \phi_3 \right)}{\cos \phi_4 \sin \left(\frac{\pi}{2} + \theta_1 - \phi_4 \right)} + \frac{t \sin \theta_1 \sin \left(\frac{\pi}{2} + \theta_2 - \phi_3 \right)}{\cos \phi_4 \sin \left(\frac{\pi}{2} + \theta_1 - \phi_4 \right) \tan \left(\frac{\pi}{2} + \theta_2 - \phi_3 \right)} + \frac{t}{\sin \left(\frac{\pi}{2} + \theta_1 - \phi_4 \right)} + \frac{z_0 z_1 z_2 z_3 z_4 \sin \theta_4}{\cos \phi_m} + \frac{t z_2 z_3 z_4 \sin \theta_4}{\cos \phi_m \tan \left(\frac{\pi}{2} + \theta_2 - \phi_1 \right)} + \frac{t z_3 z_4 \sin \theta_4}{\cos \phi_m \tan \left(\frac{\pi}{2} + \theta_1 - \phi_2 \right)} + \frac{t z_4 \sin \theta_4}{\cos \phi_m \tan \left(\frac{\pi}{2} + \theta_2 - \phi_3 \right)} + \frac{t \sin \theta_4}{\cos \phi_m \tan \left(\frac{\pi}{2} + \theta_1 - \phi_4 \right)} \right] \quad (13)$$

where, l_{odd} is the 1st bounce length of case 1 and it is between the upper surface of the converging section to the lower surface of the diverging section.

$$z_0 = \left[L_1 - x \sin \psi - \frac{x \cos \psi}{\tan(\phi_r + \psi)} \right]$$

$$z_1 = \left[1 - \frac{\sin \theta_2 \cos(\phi_r + \psi)}{\cos \phi_1} - \frac{\sin \theta_2 \sin(\phi_r + \psi)}{\cos \phi_1 \tan \left(\frac{\pi}{2} + \theta_2 - \phi_1 \right)} \right]$$

$$z_2 = \left[1 - \frac{\sin \theta_1 \cos \left(\frac{\pi}{2} + \theta_2 - \phi_1 \right)}{\cos \phi_2} - \frac{\sin \theta_1 \sin \left(\frac{\pi}{2} + \theta_2 - \phi_1 \right)}{\cos \phi_2 \tan \left(\frac{\pi}{2} + \theta_1 - \phi_2 \right)} \right]$$

$$z_3 = \left[1 - \frac{\sin \theta_2 \cos \left(\frac{\pi}{2} + \theta_1 - \phi_2 \right)}{\cos \phi_3} - \frac{\sin \theta_2 \sin \left(\frac{\pi}{2} + \theta_1 - \phi_2 \right)}{\cos \phi_3 \tan \left(\frac{\pi}{2} + \theta_2 - \phi_3 \right)} \right]$$

$$z_4 = \left[1 - \frac{\sin \theta_1 \cos \left(\frac{\pi}{2} + \theta_2 - \phi_3 \right)}{\cos \phi_4} - \frac{\sin \theta_1 \sin \left(\frac{\pi}{2} + \theta_2 - \phi_3 \right)}{\cos \phi_4 \tan \left(\frac{\pi}{2} + \theta_1 - \phi_4 \right)} \right]$$

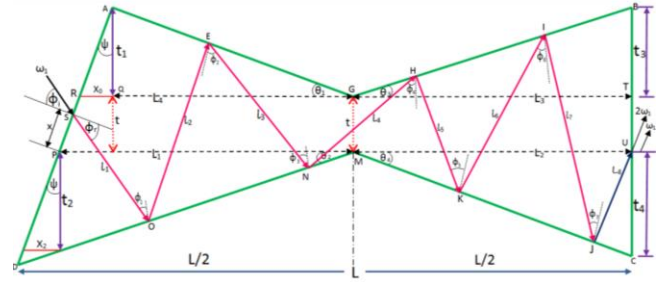


Fig. 2 Geometry of multi-tapered slab for Case 2

Now the first angle of incidence for Case 1

$$\phi_m = (\phi_1 - 4\theta_1 - 3\theta_2 + \theta_4) \quad (14)$$

For diverging section, the even and odd bounce lengths can be expressed as follows:

$$l_{even} = \left\{ \frac{D_0 \sin \theta_4 \sin \left[\frac{\pi}{2} + \theta_1 - \phi_4 - (m-2)(\theta_3 + \theta_4) \right]}{\cos \phi_{m-1} \sin \left(\frac{\pi}{2} - \theta_4 - \phi_{m-1} \right)} + \frac{t}{\sin \left(\frac{\pi}{2} - \theta_4 - \phi_{m-1} \right)} + \frac{D_{10} \sin \theta_3}{\cos \phi_m} \right\}$$

where, $m=2, 4, 6, \dots, m_{tot}$

$$\phi_{(m+1)} = [\phi_m + m(\theta_3 + \theta_4)]$$

where, $m=1, 2, 3, 4, \dots, m_{tot}$

(15)

(16)

m_{tot} indicates total number of bounces in the diverging section of multi-tapered slab.

$$\theta_3 = \tan^{-1}\left(\frac{t_3}{L_3}\right) \quad (18)$$

$$\theta_4 = \tan^{-1}\left(\frac{t_4}{L_2}\right) \quad (17)$$

$$D_0 = \left[\begin{aligned} & \frac{t}{\tan\left(\frac{\pi}{2} + \theta_1 - \phi_4\right)} - D + \frac{D \sin \theta_2 \cos(\phi_r + \psi)}{\cos \phi_1} + \frac{D \sin \theta_2 \sin(\phi_r + \psi)}{\cos \phi_1 \tan\left(\frac{\pi}{2} + \theta_2 - \phi_1\right)} \\ & + \frac{t}{\tan\left(\frac{\pi}{2} + \theta_2 - \phi_1\right)} + \frac{kj \sin \theta_1 \cos\left(\frac{\pi}{2} + \theta_2 - \phi_1\right)}{\cos \phi_2} + \frac{kj \sin \theta_1 \sin\left(\frac{\pi}{2} + \theta_2 - \phi_1\right)}{\cos \phi_2 \tan\left(\frac{\pi}{2} + \theta_1 - \phi_2\right)} \\ & + \frac{t}{\tan\left(\frac{\pi}{2} + \theta_1 - \phi_2\right)} + \frac{la \sin \theta_2 \cos\left(\frac{\pi}{2} + \theta_1 - \phi_2\right)}{\cos \phi_3} + \frac{la \sin \theta_2 \sin\left(\frac{\pi}{2} + \theta_1 - \phi_2\right)}{\cos \phi_3 \tan\left(\frac{\pi}{2} + \theta_2 - \phi_3\right)} \\ & + \frac{t}{\tan\left(\frac{\pi}{2} + \theta_2 - \phi_3\right)} + \frac{Fj \sin \theta_1 \cos\left(\frac{\pi}{2} + \theta_2 - \phi_3\right)}{\cos \phi_4} + \frac{Fj \sin \theta_1 \sin\left(\frac{\pi}{2} + \theta_2 - \phi_3\right)}{\cos \phi_4 \tan\left(\frac{\pi}{2} + \theta_1 - \phi_4\right)} \end{aligned} \right] \quad (19)$$

$$kj = \left[D - \frac{D \sin \theta_2 \cos(\phi_r + \psi)}{\cos \phi_1} - \frac{D \sin \theta_2 \sin(\phi_r + \psi)}{\cos \phi_1 \tan\left(\frac{\pi}{2} + \theta_2 - \phi_1\right)} - \frac{t}{\tan\left(\frac{\pi}{2} + \theta_2 - \phi_1\right)} \right]$$

$$la = \left[kj - \frac{kj \sin \theta_1 \cos\left(\frac{\pi}{2} + \theta_2 - \phi_1\right)}{\cos \phi_2} - \frac{kj \sin \theta_1 \sin\left(\frac{\pi}{2} + \theta_2 - \phi_1\right)}{\cos \phi_2 \tan\left(\frac{\pi}{2} + \theta_1 - \phi_2\right)} - \frac{t}{\tan\left(\frac{\pi}{2} + \theta_1 - \phi_2\right)} \right]$$

$$Fj = \left[la - \frac{la \sin \theta_2 \cos\left(\frac{\pi}{2} + \theta_1 - \phi_2\right)}{\cos \phi_3} - \frac{la \sin \theta_2 \sin\left(\frac{\pi}{2} + \theta_1 - \phi_2\right)}{\cos \phi_3 \tan\left(\frac{\pi}{2} + \theta_2 - \phi_3\right)} - \frac{t}{\tan\left(\frac{\pi}{2} + \theta_2 - \phi_3\right)} \right]$$

$$D_{10} = \left[D_0 + \frac{D_0 \sin \theta_4 \cos\left(\frac{\pi}{2} + \theta_1 - \phi_4\right)}{\cos \phi_m} + \frac{D_0 \sin \theta_4 \sin\left(\frac{\pi}{2} + \theta_1 - \phi_4\right)}{\cos \phi_m \tan\left(\frac{\pi}{2} - \theta_4 - \phi_m\right)} + \frac{t}{\tan\left(\frac{\pi}{2} - \theta_4 - \phi_m\right)} \right] \quad (20)$$

$$l_{\text{odd}} = \left[\frac{D_{10} \sin \theta_3 \sin\left(\frac{\pi}{2} - \theta_4 - \phi_{m-2}\right)}{\cos \phi_{m-1} \sin\left(\frac{\pi}{2} - \theta_3 - \phi_{m-1}\right)} + \frac{t}{\sin\left(\frac{\pi}{2} - \theta_3 - \phi_{m-1}\right)} + \frac{D_0 \sin \theta_4}{\cos \phi_m} \right] \quad (21)$$

where, $m=3, 5, 7, \dots, m_{\text{tot}}$

Case 2

$$l_{\text{even}} = \left[\begin{aligned} & \frac{z_{00} z_{10} z_{20} \sin \theta_2 \sin\left(\frac{\pi}{2} + \theta_1 - \phi_2\right)}{\cos \phi_3 \sin\left(\frac{\pi}{2} + \theta_2 - \phi_3\right)} - \frac{z_{20} \sin \theta_2 \sin\left(\frac{\pi}{2} + \theta_1 - \phi_2\right)}{\cos \phi_3 \sin\left(\frac{\pi}{2} + \theta_2 - \phi_3\right) \tan\left(\frac{\pi}{2} + \theta_2 - \phi_1\right)} \\ & - \frac{\sin \theta_2 \sin\left(\frac{\pi}{2} + \theta_1 - \phi_2\right)}{\cos \phi_3 \sin\left(\frac{\pi}{2} + \theta_2 - \phi_3\right) \tan\left(\frac{\pi}{2} + \theta_1 - \phi_2\right)} + \frac{t}{\sin\left(\frac{\pi}{2} + \theta_2 - \phi_3\right)} - \frac{z_{00} z_{10} z_{20} z_{30} \sin \theta_3}{\cos \phi_4} \\ & + \frac{t \sin \theta_3}{\cos \phi_4 \tan\left(\frac{\pi}{2} + \theta_2 - \phi_3\right)} + \frac{tz_{20} z_{30} \sin \theta_3}{\cos \phi_4 \tan\left(\frac{\pi}{2} + \theta_2 - \phi_1\right)} + \frac{tz_{30} \sin \theta_3}{\cos \phi_4 \tan\left(\frac{\pi}{2} + \theta_1 - \phi_2\right)} \end{aligned} \right] \quad (22)$$

where, l_{even} is the 1st bounce length of case 2 and it is between the lower surface of the converging section to the upper surface of the diverging section.

$$z_{00} = \left[L_1 - x \sin \psi - \frac{x \cos \psi}{\tan(\phi_r + \psi)} \right]$$

$$z_{10} = \left[1 - \frac{\sin \theta_2 \cos(\phi_r + \psi)}{\cos \phi_1} - \frac{\sin \theta_2 \sin(\phi_r + \psi)}{\cos \phi_1 \tan\left(\frac{\pi}{2} + \theta_2 - \phi_1\right)} \right]$$

$$z_{20} = \left[1 - \frac{\sin \theta_1 \cos\left(\frac{\pi}{2} + \theta_2 - \phi_1\right)}{\cos \phi_2} - \frac{\sin \theta_1 \sin\left(\frac{\pi}{2} + \theta_2 - \phi_1\right)}{\cos \phi_2 \tan\left(\frac{\pi}{2} + \theta_1 - \phi_2\right)} \right]$$

$$z_{30} = \left[1 - \frac{\sin \theta_2 \cos\left(\frac{\pi}{2} + \theta_1 - \phi_2\right)}{\cos \phi_3} - \frac{\sin \theta_2 \sin\left(\frac{\pi}{2} + \theta_1 - \phi_2\right)}{\cos \phi_3 \tan\left(\frac{\pi}{2} + \theta_2 - \phi_3\right)} \right]$$

Now the first angle of incidence for case 2,

$$\phi_m = (\phi_1 - 2\theta_1 - 3\theta_2 + \theta_3) \quad (23)$$

For diverging section, the odd and even bounce lengths can be expressed as follows:

$$l_{odd} = \left\{ \frac{D_{30} \sin \theta_3 \sin\left[\frac{\pi}{2} + \theta_2 - \phi_3 - (m-3)(\theta_3 + \theta_4)\right]}{\cos \phi_{m-1} \sin\left(\frac{\pi}{2} - \theta_3 - \phi_{m-1}\right)} + \frac{t}{\sin\left(\frac{\pi}{2} - \theta_3 - \phi_{m-1}\right)} + \frac{D_{30} \sin \theta_4}{\cos \phi_m} \right\}$$

where, $m=3, 5, 7, \dots, m_{tot}$

(24)

$$\phi_{(m+1)} = [\phi_m + m(\theta_3 + \theta_4)] \quad (25)$$

where, $m=2, 3, 4, \dots, m_{tot}$

m_{tot} indicates total number of bounces in the diverging section of multi-tapered slab.

$$D_{20} = \left[\frac{t}{\tan\left(\frac{\pi}{2} + \theta_2 - \phi_3\right)} - D + \frac{D \sin \theta_2 \cos(\phi_r + \psi)}{\cos \phi_1} + \frac{D \sin \theta_2 \sin(\phi_r + \psi)}{\cos \phi_1 \tan\left(\frac{\pi}{2} + \theta_2 - \phi_1\right)} \right]$$

$$+ \frac{t}{\tan\left(\frac{\pi}{2} + \theta_2 - \phi_1\right)} + \frac{kj \sin \theta_1 \cos\left(\frac{\pi}{2} + \theta_2 - \phi_1\right)}{\cos \phi_2} + \frac{kj \sin \theta_1 \sin\left(\frac{\pi}{2} + \theta_2 - \phi_1\right)}{\cos \phi_2 \tan\left(\frac{\pi}{2} + \theta_1 - \phi_2\right)}$$

$$+ \frac{t}{\tan\left(\frac{\pi}{2} + \theta_1 - \phi_2\right)} + \frac{la \sin \theta_2 \cos\left(\frac{\pi}{2} + \theta_1 - \phi_2\right)}{\cos \phi_3} + \frac{la \sin \theta_2 \sin\left(\frac{\pi}{2} + \theta_1 - \phi_2\right)}{\cos \phi_3 \tan\left(\frac{\pi}{2} + \theta_2 - \phi_3\right)} \quad (26)$$

$$D_{30} = \left[D_{20} + \frac{D_{20} \sin \theta_3 \cos\left(\frac{\pi}{2} + \theta_2 - \phi_3\right)}{\cos \phi_m} + \frac{D_{20} \sin \theta_3 \sin\left(\frac{\pi}{2} + \theta_2 - \phi_3\right)}{\cos \phi_m \tan\left(\frac{\pi}{2} - \theta_3 - \phi_m\right)} + \frac{t}{\tan\left(\frac{\pi}{2} - \theta_3 - \phi_m\right)} \right] \quad (27)$$

$$kj = \left[D - \frac{D \sin \theta_2 \cos(\phi_r + \psi)}{\cos \phi_1} - \frac{D \sin \theta_2 \sin(\phi_r + \psi)}{\cos \phi_1 \tan\left(\frac{\pi}{2} + \theta_2 - \phi_1\right)} - \frac{t}{\tan\left(\frac{\pi}{2} + \theta_2 - \phi_1\right)} \right]$$

$$la = \left[kj - \frac{kj \sin \theta_1 \cos\left(\frac{\pi}{2} + \theta_2 - \phi_1\right)}{\cos \phi_2} - \frac{kj \sin \theta_1 \sin\left(\frac{\pi}{2} + \theta_2 - \phi_1\right)}{\cos \phi_2 \tan\left(\frac{\pi}{2} + \theta_1 - \phi_2\right)} - \frac{t}{\tan\left(\frac{\pi}{2} + \theta_1 - \phi_2\right)} \right]$$

$$l_{even} = \left\{ \frac{D_{30} \sin \theta_4 \sin\left(\frac{\pi}{2} - \theta_3 - \phi_{m-2}\right)}{\cos \phi_{m-1} \sin\left(\frac{\pi}{2} - \theta_4 - \phi_{m-1}\right)} + \frac{t}{\sin\left(\frac{\pi}{2} - \theta_4 - \phi_{m-1}\right)} + \frac{D_{20} \sin \theta_3}{\cos \phi_m} \right\}$$

where, $m=4, 6, 8, \dots, m_{tot}$

(28)

Thus the total number of bounces inside the multi-tapered slab can be found by the sum of n_{tot} and m_{tot} .

2.2. Polarization aspect

In our analysis, we have dealt with ppp polarization for ZnTe and CdTe isotropic crystal. The value of d_{14} is considered to be 90 pm/V [12] for ZnTe and 170 pm/V for CdTe [11].

2.3. Rayleigh range

Here, the total interaction length (L_{tot}) has been obtained by adding up all the bounce lengths inside the ZnTe and CdTe slab for the center wavelengths 10.737 μm and 7.85 μm of the fundamental beam which comes around 1.2 cm for ZnTe and 1.3 cm for CdTe. The Rayleigh range when calculated for the same wavelength, assuming a beam waist of 100 μm comes out to be 1.57 cm for ZnTe and 2.14 cm for CdTe, which is greater than L_{tot} .

2.4. Conversion yield limiting factors

The SHG conversion efficiency is restricted by 3 significant factors; these are surface roughness, GH shift and linear absorption.

(i) The surface roughness causes a scattering of the light at reflection which in turn leads to a drop of the TIR coefficient [9]. This effect has been simulated assuming a p-v value of 30 nm for both ZnTe [13] and CdTe. (ii) The GH shift causes a reduction of the usable length of the semiconductor slab [14]. In our proposed slab the GH shift has been calculated for both upper and lower tapered surfaces of the converging as well as diverging section. (iii) Linear absorption has deteriorating effect on SHG due to heating of the material. In our case, we have considered a linear absorption coefficient ($\alpha_{\omega_0} \approx \alpha_{2\omega_0}$) of 0.008 cm^{-1} for selected ZnTe [15] and 0.0014 cm^{-1} for CdTe material [16].

2.5. Study of nonlinear law of reflection

As noted by Bloembergen et al. [17] due to nonlinear reflection at each TIR bounce point, we get two SH waves, i.e., homogeneous SH wave and collinear SH wave. There

will be a certain angular separation between the two waves which can be expressed as,

$$\delta\phi \approx -\left(\frac{\delta n}{n}\right) \tan \phi_o \quad (29)$$

Here, $\delta n = n_{2\omega} - n_{\omega}$ is the optical dispersion

Now, for parallel slab if the separation between collinear SH and homogeneous SH is increasing then it leads to 2 effects: (i) spatial walk-off which reduces the overlap between the beams. (ii) the pump and parametric beams may recombine after a certain number of bounces then generated beam fills the plate completely. This recombination may lead to destructive interferences [18]. In case of our proposed slab, it follows the same principle where we get the two SH wave and they are travelling with an angular shift of $\delta\phi_n$. Here, the SH field of first bounce point will undergo a Fresnel phase shift at next bounce and will contribute to the newly generated SH at that bounce point. The same process will be repeated at the next bounce point and so on. Finally, we will obtain the net electric field by summing all the homogeneous SHs as well as the collinear SHs generated inside the multi-tapered slab. The effect of spatial walk-off suggested by Smith et al. [19] has been calculated using the term,

$$\left[\frac{1}{\sqrt{1+0.51(\rho L/W)^2}} \right]$$

2.6. SH conversion efficiency

The SH conversion efficiency is given by:

$$\eta_{con} = \left[\frac{S_2}{S_1} \times 100\% \right] \quad (30)$$

where, S_2 is the output SH intensity and S_1 is the fundamental beam intensity [20].

3. Results and discussions

The SH conversion efficiency with respect to the fundamental wavelength has been studied with the help of the computer-aided simulation for both ZnTe and CdTe and it as shown in Fig. 3 and Fig. 4 respectively. In this simulation, we have used a fundamental broadband source of 10-12 μm for ZnTe and 7-9 μm for CdTe and the input beam intensity is assumed to be $S_1 = 10 \text{ MW/cm}^2$.

3.1. Effect of variation in slab length

Table 1 and 2 respectively shows the results for slab length variation in ZnTe and CdTe. Here, we can see that with increase in slab length, SH conversion efficiency increases with a drop in BW.

3.2. Effect of variation in vertical heights of both the sections (t_1, t_2, t_3, t_4)

Table 3 and 4 shows the variation in t_1 for ZnTe and CdTe respectively. Table 5 and 6 shows the variation in t_2 . Table 7 and 8 shows the variation in t_3 . Table 9 and 10 shows the variation in t_4 .

3.3. Effect of different losses

The effects of linear absorption, GH shift surface roughness and nonlinear law of reflection on both the fundamental wave and the SH wave are considered and it is shown in Fig. 15 and 16.

The simulated results indicates-For ZnTe, the SH conversion efficiency of 11.34 % while the 3 dB BW of 426 nm and it is for ideal condition. When the optical losses are considered the peak conversion efficiency reduces to 6.87 % while the 3 dB BW of 462 nm and the usable slab length is reduced by 0.043 mm due to the effect of GH shift.

For CdTe, under ideal condition a SH conversion efficiency of 22.37 % while the 3 dB BW of 346 nm. When the optical losses are considered the peak conversion efficiency reduces to 8.46 % while the 3 dB BW of 358 nm and the usable slab length is reduced by 0.045 mm due to the effect of GH shift.

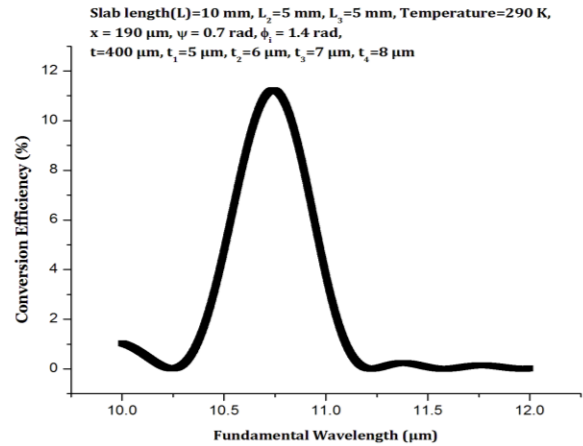


Fig. 3 Variation of SH efficiency with respect to fundamental wavelength for the multi-tapered slab (ZnTe)

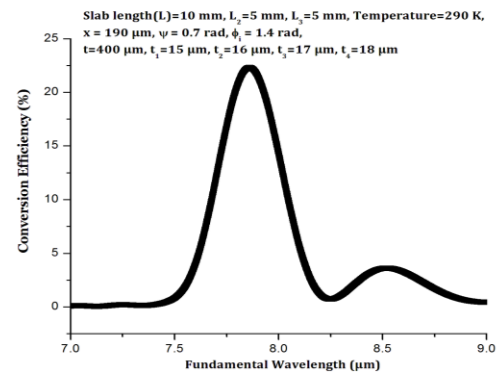


Fig. 4. Variation of SH efficiency with respect to fundamental wavelength for the multi-tapered slab (CdTe)

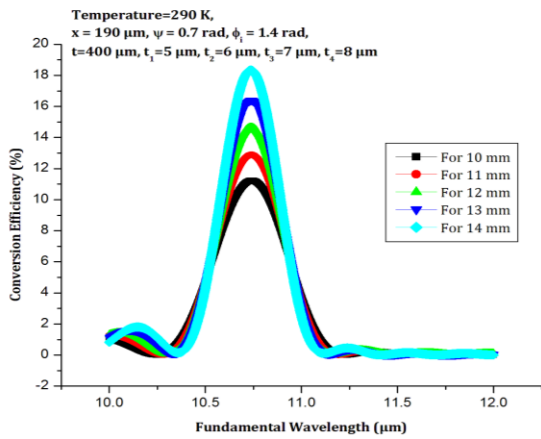


Fig. 5 Variation of SH efficiency with respect to fundamental wavelength, as a function of slab length L for ZnTe.

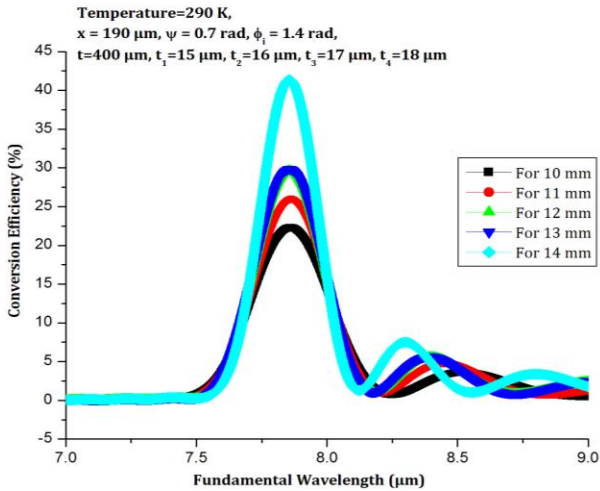


Fig. 6. Variation of SH efficiency with respect to fundamental wavelength, as a function of slab length L for CdTe.

Table 1. Effect of variation in slab length (L) for ZnTe where the other parameters are constant i.e. temperature = 290 K, $\psi = 0.7$ rad, $\phi_1 = 1.4$ rad, $t = 400$ μm , $t_1 = 5$ μm , $t_2 = 6$ μm , $t_3 = 7$ μm , $t_4 = 8$ μm

Material	Slab length (mm)	Peak conversion efficiency (%)	Centre wavelength of fundamental (μm)	3 dB bandwidth (nm)
ZnTe	0	11.34	10.737	426
	1	12.99	10.730	404
	2	14.74	10.739	375
	3	16.55	10.735	361
	4	18.42	10.737	332

Table 2. Effect of variation in slab length (L) for CdTe where the other parameters are constant i.e. temperature = 290 K, $\psi = 0.7$ rad, $\phi_1 = 1.4$ rad, $t = 400$ μm , $t_1 = 15$ μm , $t_2 = 16$ μm , $t_3 = 17$ μm , $t_4 = 18$ μm

Material	Slab length (mm)	Peak conversion efficiency (%)	Centre wavelength of fundamental (μm)	3 dB bandwidth (nm)
CdTe	0	22.37	7.858	346
	1	25.96	7.857	317
	2	29.34	7.857	303
	3	29.82	7.857	303
	4	41.41	7.848	260

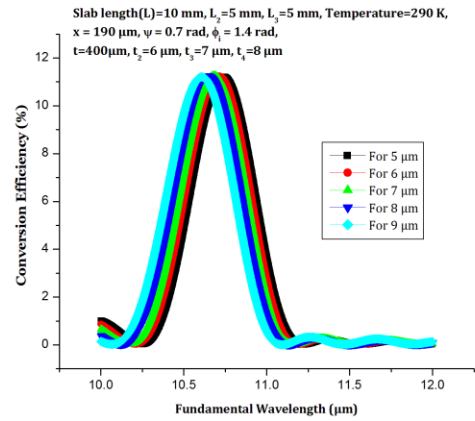


Fig. 7. Variation of SH efficiency with respect to fundamental wavelength, as a function of t_1 for ZnTe

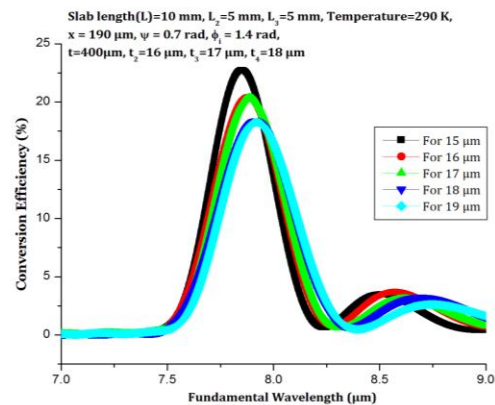


Fig. 8 Variation of SH efficiency with respect to fundamental wavelength, as a function of t_1 for CdTe.

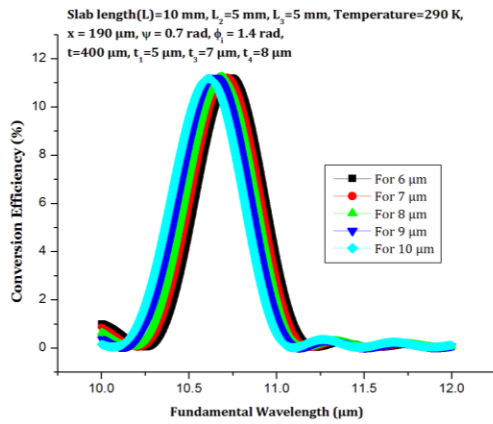


Fig. 9. Variation of SH efficiency with respect to fundamental wavelength, as a function of t_2 for ZnTe.

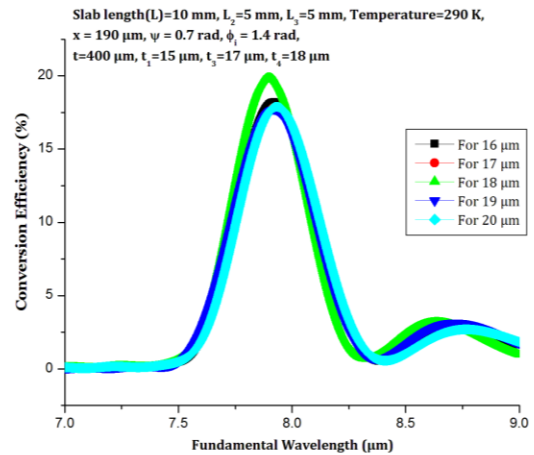


Fig. 10. Variation of SH efficiency with respect to fundamental wavelength, as a function of t_2 for CdTe.

Table 3. Effect of variation in vertical height (t_1) for ZnTe, where the other parameters are constant i.e. Slab length $L = 10$ mm, $L_2 = 5$ mm, $L_3 = 5$ mm, $\psi = 0.7$ rad, $\phi_1 = 1.4$ rad, $t = 400$ μ m, $t_2 = 6$ μ m, $t_3 = 7$ μ m, $t_4 = 8$ μ m.

Material	t_1 (μ m)	Peak conversion efficiency (%)	Centre wavelength of fundamental (μ m)	3 dB bandwidth (nm)
ZnTe	5	11.34	10.737	426
		11.30	10.707	433
		11.30	10.678	440
		11.28	10.643	440
		11.28	10.603	447

Table 4. Effect of variation in vertical height (t_1) for CdTe, where the other parameters are constant i.e. Slab length $L = 10$ mm, $L_2 = 5$ mm, $L_3 = 5$ mm, $\psi = 0.7$ rad, $\phi_1 = 1.4$ rad, $t = 400$ μ m, $t_2 = 16$ μ m, $t_3 = 17$ μ m, $t_4 = 18$ μ m.

Material	t_1 (μ m)	Peak conversion efficiency (%)	Centre wavelength of fundamental (μ m)	3 dB bandwidth (nm)
CdTe	15	22.37	7.858	346
	16	20.41	7.876	375
	17	20.36	7.876	361
	18	18.38	7.912	404
	19	18.28	7.912	418

Table 5. Effect of variation in vertical height (t_2) for ZnTe, where the other parameters are constant i.e. Slab length, $L = 10$ mm, $L_2 = 5$ mm, $L_3 = 5$ mm, $\psi = 0.7$ rad, $\phi_1 = 1.4$ rad, $t = 400$ μ m, $t_1 = 5$ μ m, $t_3 = 7$ μ m, $t_4 = 8$ μ m.

Material	t_2 (μ m)	Peak conversion efficiency (%)	Centre wavelength of fundamental (μ m)	3 dB bandwidth (nm)
ZnTe	6	11.30	10.737	426
		11.30	10.717	440
		11.32	10.682	433
		11.25	10.647	447
	10	11.21	10.610	447

Table 6. Effect of variation in vertical height (t_2) for CdTe, where the other parameters are constant i.e. Slab length, $L = 10$ mm, $L_2 = 5$ mm, $L_3 = 5$ mm, $\psi = 0.7$ rad, $\phi_1 = 1.4$ rad, $t = 400$ μ m, $t_1 = 15$ μ m, $t_3 = 17$ μ m, $t_4 = 18$ μ m.

Material	t_2 (μ m)	Peak conversion efficiency (%)	Centre wavelength of fundamental (μ m)	3 dB bandwidth (nm)
CdTe	16	22.37	7.858	346
	17	17.92	7.931	404
	18	19.79	7.899	375
	19	17.71	7.912	404
	20	17.92	7.931	390

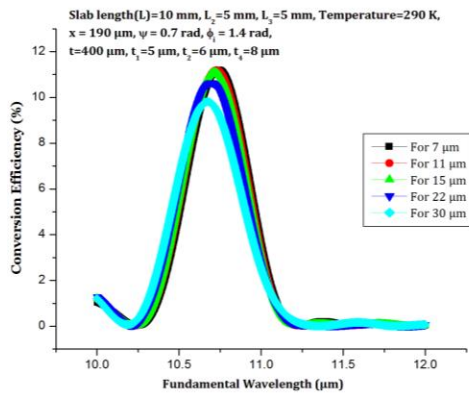


Fig. 11 Variation of SH efficiency with respect to fundamental wavelength, as a function of t_3 for ZnTe.

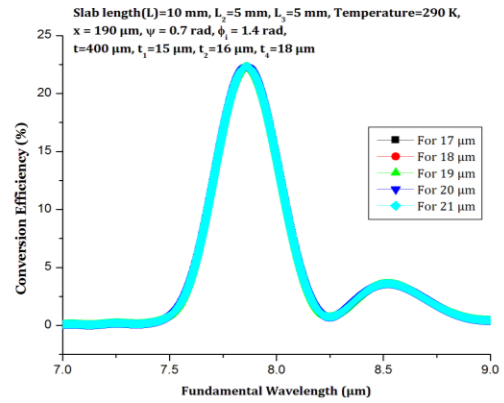


Fig. 12 Variation of SH efficiency with respect to fundamental wavelength, as a function of t_3 for CdTe.

Table 7. Effect of variation in vertical height (t_3), where the other parameters are constant i.e. Slab length, $L = 10 \text{ mm}$, $L_2 = 5 \text{ mm}$, $L_3 = 5 \text{ mm}$, $\psi = 0.7 \text{ rad}$, $\phi_1 = 1.4 \text{ rad}$, $t = 400 \text{ }\mu\text{m}$, $t_1 = 5 \text{ }\mu\text{m}$, $t_2 = 6 \text{ }\mu\text{m}$, $t_4 = 8 \text{ }\mu\text{m}$.

Material	t_3 (μm)	Peak conversion efficiency (%)	Centre wavelength of fundamental (μm)	3 dB bandwidth (nm)
ZnTe	7	11.34	10.737	426
	11	11.28	10.722	426
	15	11.14	10.712	426
	22	10.71	10.690	440
	30	9.86	10.670	455

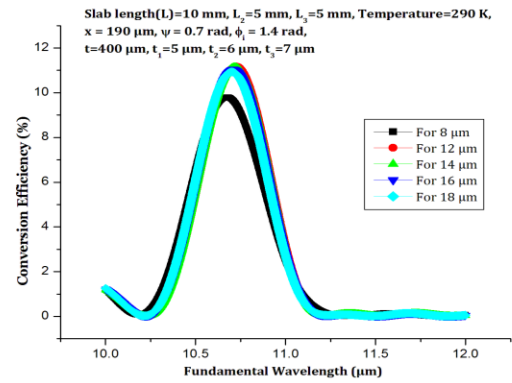


Fig. 13 Variation of SH efficiency with respect to fundamental wavelength, as a function of t_4 for ZnTe.

Table 8. Effect of variation in vertical height (t_3) for CdTe, where the other parameters are constant i.e. Slab length, $L=10 \text{ mm}$, $L_2 = 5 \text{ mm}$, $L_3 = 5 \text{ mm}$, $\psi = 0.7 \text{ rad}$, $\phi_1 = 1.4 \text{ rad}$, $t = 400 \text{ }\mu\text{m}$, $t_1 = 15 \text{ }\mu\text{m}$, $t_2 = 16 \text{ }\mu\text{m}$, $t_4 = 18 \text{ }\mu\text{m}$.

Material	t_3 (μm)	Peak conversion efficiency (%)	Centre wavelength of fundamental (μm)	3 dB bandwidth (nm)
CdTe	17	22.37	7.858	346
	18	22.27	7.857	332
	19	22.27	7.857	332
	20	22.33	7.857	332
	21	22.27	7.857	332

Table 9. Effect of variation in vertical height (t_4), where the other parameters are constant i.e. Slab length, $L = 10 \text{ mm}$, $L_2 = 5 \text{ mm}$, $L_3 = 5 \text{ mm}$, $\psi = 0.7 \text{ rad}$, $\phi_1 = 1.4 \text{ rad}$, $t = 400 \text{ }\mu\text{m}$, $t_1 = 5 \text{ }\mu\text{m}$, $t_2 = 6 \text{ }\mu\text{m}$, $t_3 = 7 \text{ }\mu\text{m}$

Material	t_4 (μm)	Peak conversion efficiency (%)	Centre wavelength of fundamental (μm)	3 dB bandwidth (nm)
ZnTe	8	11.34	10.737	426
	12	11.25	10.722	426
	14	11.18	10.715	440
	16	11.14	10.707	433
	18	11.00	10.702	433

Table 10. Effect of variation in vertical height (t_4) for CdTe, where the other parameters are constant i.e. Slab length, $L=10$ mm, $L_2=5$ mm, $L_3=5$ mm, $\psi=0.7$ rad, $\phi_1=1.4$ rad, $t=400$ μ m, $t_1=15$ μ m, $t_2=16$ μ m, $t_{43}=17$ μ m.

Material	t_4 (μ m)	Peak conversion efficiency (%)	Centre wavelength of fundamental (μ m)	3 dB bandwidth (nm)
CdTe	17	22.37	7.858	346
	18	22.27	7.867	346
	19	22.27	7.867	346
	20	22.27	7.867	346

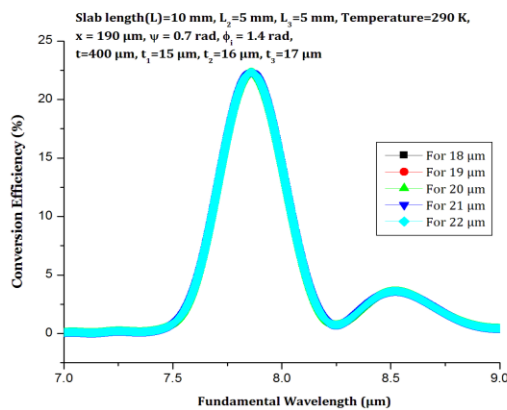


Fig. 14 Variation of SH efficiency with respect to fundamental wavelength, as a function of t_4 for CdTe

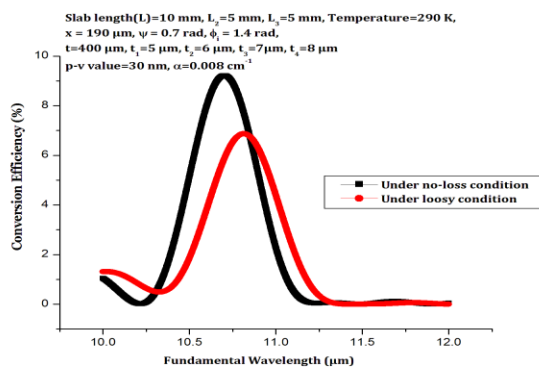


Fig. 15 Variation of SH conversion efficiency with respect to the fundamental wavelength under ideal and lossy condition for ZnTe

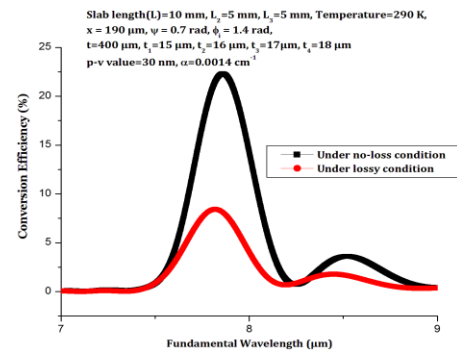


Fig. 16 Variation of SH conversion efficiency with respect to the fundamental wavelength under ideal and lossy condition for CdTe.

4. Conclusion

We have numerically analyzed a broadband frequency converter using a ZnTe and CdTe multi-tapered slab configuration based on TIR-QPM. The proposed converter provides a wide bandwidth of 426 nm with a peak conversion efficiency of 11.34 % and 346 nm with a efficiency 22.37 % for ZnTe and CdTe respectively. When the all losses has been considered, the SH efficiency reduces to 6.87 % while the 3 dB bandwidth increases by 36 nm and 8.46% while the 3 dB bandwidth increases by 12 nm for ZnTe and CdTe respectively. Hence the proposed configuration reveals itself as a highly efficient broadband frequency converter which in turn can be used in IR spectroscopy [17] and thermal imaging, particularly in the mid infrared region.

References

- [1] M. M. Fejer, G. A. Magel, E. J. Lim, Proc. SPIE, Nonlinear Optical Properties of Materials **1148**, 213 (1990).
- [2] K. Mizuuchi, K. Yamamoto, Appl. Phys. Lett. **60**, 1283 (1992).
- [3] E. Rosencher, Towards integrated semiconductor optical parametric oscillators, C. R. Acad. Sci. Paris, Series IV, 615 (2000).
- [4] M. B. Raybaut, R. Haidar, Ph. Kupecek, Ph. Lemasson E. Rosencher, Nature **432**, 374 (2004).
- [5] R. L. Sutherland, Handbook of Nonlinear Optics, Marcel Dekker, New York, (1996).
- [6] J. A. Armstrong, N. Bloembergen, J. Ducuing, P. S. Pershan, Phys. Rev. **127**, 1918 (1962).
- [7] G. D. Boyd, C. K. N. Patel, Appl. Phys. Lett. **8**, 313 (1966).
- [8] H. Komine, W. H. Long Jr., J.W. Tully, E. A. Stappaerts, Opt. Lett. **23**, 661 (1998).

- [9] R. Hadar, N. Forget, P. Kupecek, E. Rosencher, *J. Opt. Soc. Am. B* **21**, 1522 (2004).
- [10] H. H. Li, *J. Phys. Chem. Ref. Data* **13**, 103 (1984).
- [11] http://extras.springer.com/2005/978-3-540-44376-6/10678245/10678245-c_44/10678245-c-4-4.pdf
- [12] S. Deb, A. Saha, *Optik-International Journal for Light and Electron Optics* **124**, 2428 (2013).
- [13] N. Lovergine, D. Manno, A. M. Mancini L. Vasanelli, *J. Cryst. Growth* **128**, 633 (1993).
- [14] A. Saha, S. Deb, *Opt. Commun.* **284**, 4714 (2011).
- [15] [http://www.optoscience.com/maker/gooch/pdf/II-VI\(CdS\)](http://www.optoscience.com/maker/gooch/pdf/II-VI(CdS))
- [16] A. W. Tucker, M. Birnbaum, H. Montes, C. L. Fincher, *Applied Optics* **21**, 1490 (1982).
- [17] N. Bloembergen and P. S. Pershan, *Phys. Rev.* **128**, 606 (1962).
- [18] M. Raybaut, A. Godard, A. Toulouse, C. Lubin, E. Rosencher, *Opt. Exp.* **16**, 18457 (2008).
- [19] A. V. Smith, D. J. Armstrong, W. J. Alford, *J. Opt. Soc. Am. B* **15**, 122 (1998).
- [20] S. Banik, U. Das, S. Deb, A. Saha, *Opt. Commun.* **295**, 180 (2013).

*Corresponding author: sumitanitae@gmail.com